Materials Advances

ROYAL SOCIETY OF CHEMISTRY

PAPER

View Article Online
View Journal | View Issue

Check for updates

Cite this: *Mater. Adv.*, 2022, 3, 4600

Novel optical amorphous phosphate materials with a low melting temperature

Simon Kaser,[ab] Théo Guérineau,[*b] Clément Strutynski,[a] Reda Zaki,[a] Marc Dussauze,[c] Etienne Durand,[a] Sandra H. Messaddeq,[b] Sylvain Danto,[a] Younès Messaddeq[b] and Thierry Cardinal[a]

Received 26th October 2021,
Accepted 17th April 2022

DOI: 10.1039/d1ma00995h

rsc.li/materials-advances

We report on the synthesis of transparent amorphous hydrated phosphate materials at low temperatures (as low as 300 °C) in the $\left[50P_2O_5 - \left(25 - \frac{x}{2}\right)K_2O - \left(25 - \frac{x}{2}\right)Na_2O - xZnO\right] - nH_2O$ (0–25 mol%). These new transparent materials were studied by Raman and FTIR spectroscopies. The structure of the hydrated phosphates is proposed to consist of both short phosphate chains and isolated phosphate groups linked together by hydrogen bonds. Containing up to 40 mol% of water, most of the physico-chemical properties remain unchanged, except for the characteristic glass temperatures. Moreover, the most hydrated amorphous phosphate materials tend to exhibit a softening phenomenon below 150 °C. The addition of ZnO to these phosphate materials offers better glass stability against moisture while maintaining the glass properties of zinc-free materials. Hence, these new amorphous transparent materials pave the way for novel low melting temperature optical materials.

Introduction

One of the most limiting aspects of the development of optical glass-based or glass-containing composite materials is their high fabrication temperature. Indeed, even though the introduction of a large amount of either network modifiers (such as alkali or alkaline-earth ions) or halogen ions in the vitreous material helps reduce significantly both glass transition and melting temperatures, it also drastically affects the physico-chemical properties of the glass. Thus, for decades, the most conventional way to synthesize low-melting glasses has been the introduction of lead oxide in the glass composition.[1] However, many countries have since then forbidden the use of lead due to its hazardousness for both the environment and human body.

Among amorphous optical materials, phosphate matrices are reported to exhibit much lower glass transition temperatures than common silicate glass compositions. Their broad varieties of compositions possessing good thermal and chemical stabilities, and interesting optical properties have led to their employment in fiber-drawing or 3D printing applications.[2,3] Although phosphate glasses are also known for their poor chemical durability, such limitations can be overcome efficiently by tailoring the glass matrix with metallic cations such as Al^{3+} or Zn^{2+}. The structure of phosphate glasses is based on the arrangement of tetrahedral units classified by using the Q^n terminology, where n refers to the number of bridging oxygens per tetrahedron. Therefore, depending on the oxygen over phosphorus ratio (O/P), the glass structure consists of either cross-linked networks of Q^3 tetrahedra (O/P < 3), polyphosphate chains of Q^2 tetrahedra (3 < O/P < 3.5), invert glasses with Q^1 pyrophosphate units composed of two tetrahedra (3.5 < O/P < 4), or finally isolated Q^0 orthophosphate units (O/P = 4).[4]

As reported by Popova and Dimitriev in their review on tin-based amorphous materials, oxyfluoride or oxychloride phosphate glasses containing SnF_2 or $SnCl_2$ can have glass transition temperatures below 100 °C.[5] However, the preparation of such materials remains complicated, since a strict control of the atmosphere is required during the glass synthesis to maintain the oxidation degree of tin, avoiding the formation of metal Sn or SnO_2. Even if the durability towards moisture remains poor, Masai *et al.* have recently reported that tin-containing phosphate glasses could exhibit higher thermal and better resistance to UV light degradation than polycarbonates.[6]

Soft chemistry offers the opportunity to assemble materials of exotic nature *via* low-temperature processing.[7–9] Considerable efforts have already been devoted to silica-based materials to significantly reduce fabrication temperatures using for instance the sol–gel process.[10,11] Another glass synthesis route based on hydrated materials is also of great interest. In the case of optical crystalline compounds, the well-known potassium dihydrogen phosphate compound (also known as KDP of

[a] CNRS, Université de Bordeaux, Bordeaux INP, ICMCB, UMR 5026, F-33600 Pessac, France
[b] Centre d'Optique, Photonique et Laser (COPL), Université Laval, Québec, QC, Canada. E-mail: theo.guerineau@gmail.com
[c] CNRS, Université de Bordeaux, ISM, UMR-5255, Talence F-33405, France

chemical formula KH_2PO_4) has shown excellent transparency and second-order optical nonlinearity.[12–14] These interesting properties have led to numerous applications including the fabrication of large optical components in laser fusion facilities even if its fast crystalline growth process remains highly challenging.[15]

Soft chemistry methods involving hydrated phosphate synthesis have recently drawn attention in a variety of fields from cement engineering to biomaterial and energy applications.[16–19] Among them, one can mention the chemical reaction *via* coacervation that has been applied for electrical sealing or biomaterial applications.[20,21] Starting from a Graham salt ($Na(PO_3)_n$) solution, the coacervation process consists of promoting the liquid–liquid phase separation thanks to the presence of long phosphate chains which leads to the formation of a phosphate gel called ''coacervate'' and a supernatant phase. Recently, *via* an electrospinning step at room temperature, Foroutan *et al.* reported the formation of a phosphate-base amorphous cotton-like material from a phosphate coacervate.[22] The final amorphous material was prepared at room temperature; however, it cannot be used for optical applications since the final compound was not a transparent bulk material. With a similar synthesis route, Orives *et al.* reported on the conception of a functionalized phosphate-based coacervate with $CdFe_2O_4$ nanoparticles.[23] However, a final melt-quenching step at high temperature (above 800 °C) remained necessary to obtain the final optical material. Hence, and as previously highlighted by several authors before, the coacervation route allows mainly the preparation of phosphate-based optical glass precursors but is not yet able to provide optical transparent materials.[24]

Water-containing phosphate glasses have also been reported in the literature. Nepomuliev *et al.* studied glasses in the Na_2SO_4–P_2O_5–H_2O system, with a water content determined by ^1H NMR to be as high as 10 mol%.[25] Mercier *et al.* highlighted the structure of hydrated zinc ultraphosphate glasses,[26] while Ehrt investigated the effect of OH-content, up to 20 mol%, on the structure and properties of SnO–P_2O_5 glasses, with T_g around 150–200 °C.[27]

Herein, we present the fabrication at low temperatures (as low as 300 °C) of transparent amorphous phosphate materials in the system P_2O_5–K_2O–Na_2O–ZnO–H_2O. A structural investigation of these amorphous hydrated phosphates was performed to determine the network structure of these atypical materials, by means of Raman and infrared spectroscopies. The structure and properties of hydrated phosphates were also compared to those of phosphate glasses of similar compositions obtained using a classical high-temperature melt-quenching technique.

Experimental section

Material syntheses

Hydrated phosphate materials were synthesized using the melt-quenching technique at different temperatures (300 °C, 500 °C and 800 °C). Powder precursors (K_2CO_3, 98%, Roth; Na_2CO_3, 99%, Roth; ZnO, 99.9%, Alfa Aesar; Eu_2O_3, 99.9%, Alfa Aesar) were weighed in adequate molar ratios and mixed in a Teflon beaker. An adequate amount of H_3PO_4, from water-diluted phosphoric acid solution (85%, Roth), was weighed and poured slowly into the Teflon beaker while thoroughly stirring the mixture. The mixture was heat-treated in a sand bath at approximately 250 °C for 16 h. The resulting solid compound was ground and heated at 300 °C in a vitreous carbon crucible for 1 h while maintaining stirring to ensure the homogeneity of the liquid. The melt was then poured into a steel mold at room temperature. For treatments at 500 °C and 800 °C, the materials obtained from the sand bath treatment were heated in a platinum crucible for 1 h and poured in a steel mold. No reactions between the vitreous carbon or platinum crucibles and the intermediate compound were observed. To perform the optical measurements requiring a good optical quality, the two parallel faces of each sample were optically polished with isopropanol. However, for samples with less than 15 mol% of ZnO, the optical polishing could not be easily obtained due to their high hygroscopicity. All samples were stored in a vacuum desiccator to prevent any ageing process.

Material characterization

Thermal analysis was performed by differential thermal analysis (DTA) using a Netzsch DSC 404. Approximately 60 mg of bulk material were inserted in an alumina pan and placed in a chamber with an empty reference pan. The scans were performed from room temperature to 500 °C at a 10 °C min^{-1} rate. Thermogravimetric analysis was performed using a SETARAM Setsys Evolution under a 50 mL min^{-1} Argon gas flow. The samples were inserted in a platinum pan and the analysis was performed from room temperature to 800 °C at a 5 °C min^{-1} rate. Estimation of the durability of glass samples was carried out through weight loss measurements after immersion in deionized water at room temperature. Accordingly, the dissolution rate was calculated as the slope between zero and the final data point. Roughly polished bulk slabs were used for these measurements.

Raman spectra were recorded using a LABRAM 800-HR spectrometer (Horiba Jobin-Yvon) with a resolution of 2.5 cm^{-1} in the 400–4000 cm^{-1} wavenumber range at room temperature with a single longitudinal mode laser emitting at 532 nm as the excitation source.

Infrared spectra were recorded using a Bruker VERTEX 70v and a DLaTGS detector on samples polished with isopropanol, operating under vacuum in specular reflectance mode with an 8 cm^{-1} spectral resolution. A total of 200 scans were performed in the 7000 cm^{-1}–100 cm^{-1} range. The recorded spectra were analyzed by the Kramers–Kronig transformation to obtain the absorption coefficient spectra, $\alpha(\nu)$.

The emission and excitation spectra of rare-earth-doped samples were recorded at room temperature with an Edinburgh Instruments spectrofluorometer, using a Xenon lamp as the excitation source and with a PMT detector. The density of the materials was measured at room temperature through Archimedes' method in diethyl phthalate (Sigma Aldrich) with an accuracy of 0.02 g cm^{-3}.

Refractive indices were measured at 480, 589, 644 and 656 nm using a DR-M4 Abbe refractometer (Atago, Japan) with a ± 0.01 precision.

The optical transmission curves were recorded using an Agilent Cary 5000 spectrometer in the spectral range of 1500–200 nm with a step of 1 nm and an integration time of 0.1 s.

Results

Hydrated phosphate materials of the composition $(1 - x)(50P_2O_5–25K_2O–25\ Na_2O)–xH_2O$ were first synthetized. Zinc oxide was then added to the precursors in substitution of potassium and sodium oxides. The nominal compositions of investigated oxide compounds are shown in Table 1 without considering the water content, which is introduced in large excess (more than half of the entire compound in molar content). In the case of the europium-doped material P50Zn25Eu, 0.1 mol% of Eu_2O_3 was introduced. The materials were prepared at three fixed temperatures: 300 °C, 500 °C and 800 °C. Transparent materials were obtained for all compositions with up to 25 mol% of ZnO at 300 °C, 500 °C and 800 °C. The chemical stability of both P50 and P50Zn25 samples made at 300 °C has been succinctly evaluated under UV light exposure for 65 hours and in a deionized water dissolution. After UV light exposure no glass modifications were reported on both glasses, while during the water dissolution a 4 times higher resilience was denoted for the P50Zn25 (7.7×10^{-3} g cm^{-2} min^{-1}) than for the P50 (1.4×10^{-2} g cm^{-2} min^{-1}). Glasses prepared at 300 °C are very hygroscopic and tend to rapidly deteriorate when stored in contact with normal atmosphere. However, these glasses were not affected when stored in a desiccator for more than three months.

P50 materials prepared at two different temperatures, *i.e.*, 300 °C and 800 °C are presented in Fig. 2(a). Both samples are amorphous and transparent, as demonstrated by the X-ray diffractogram (Fig. 2(b)) and transmission curve (Fig. 2(c)), respectively. The absorption edge observed at about 325 nm corresponds only to the absorption of both borosilicate glass coverslips.

To evaluate the water and/or hydroxyl group content in the resulting materials, a thermogravimetric analysis was performed. Fig. 1 presents the TGA results for two hydrated phosphate samples prepared at 300 °C, the first one with no addition of ZnO (P50) and the second one with 25 mol% of ZnO (P50Zn25). Three main mass loss events are recorded here for both samples. The first one, between 65 °C and 150 °C, corresponds to the loss of 0.5% and 0.8% for samples P50 and P50Zn25, respectively. Then, two events are recorded above 300 °C. From 300 °C to 440 °C, a sharp decrease (−8.7%) can be seen for the P50 sample, followed by a minor mass loss (−0.5%) from 450 °C to 530 °C. While for sample P50Zn25, these mass losses are less pronounced: −3.6% between 300 °C and 400 °C, −2.6% between 400 °C and 520 °C, and −0.8% between 520 °C and 650 °C. The total mass loss measured at 700 °C is 11.5% for sample P50 and 9% for sample P50Zn25. The water content at 800 °C is negligible and estimated to be less than 1%. The estimated measured compositions of the materials at 300, 500 and 800 °C with the water content were calculated from the mass loss values and are reported in Table 2.

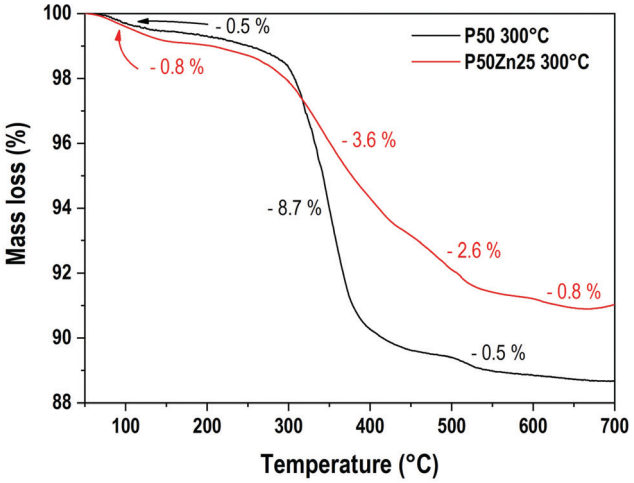

Fig. 1 TGA curves of the P50 and P50Zn25 samples synthesized at 300 °C.

Table 1 Nominal contents (mol%) of the hydrated zinc phosphates

Label	Nominal contents (mol%)				
	P_2O_5	K_2O	Na_2O	ZnO	Eu_2O_3
P50	50	25	25	—	—
P50Zn5	50	22.5	22.5	5	—
P50Zn10	50	20	20	10	—
P50Zn15	50	17.5	17.5	15	—
P50Zn20	50	15	15	20	—
P50Zn25	50	12.5	12.5	25	—
P50Zn25Eu	50	12.5	12.5	24.9	0.1

The DTA curves for the P50 composition prepared at 300 °C, 500 °C and 800 °C are presented in Fig. 3. The baseline was measured by performing the same operation with the same empty alumina crucible and subsequently subtracted to the recorded signal. The sample prepared at 800 °C shows a glass transition phenomenon located at 210 °C, an exothermic event at 380 °C corresponding to the crystallization temperature and an endothermic peak at 537 °C which corresponds to the melting temperature. The glass transition temperature recorded is in good accordance with the value already reported in the literature at 215 °C for a sodium–potassium phosphate glass with 54 mol% of phosphorus and 46 mol% of sodium and potassium in equimolar proportion.[28] The sample prepared at 500 °C also presents a glass transition at 150 °C as well as two exothermic events around 280 °C and 350 °C. Above 500 °C, the increase of the DTA signal matches the temperature corresponding to the water losses detected earlier in TGA.

Regarding the sample prepared at 300 °C, an event can be observed around 100 °C. It is unclear whether this event could be related to the elimination of water or a glass transition phenomenon. Another exothermic event is observed starting at 320 °C, which is comparable to the one observed at 500 °C for the sample prepared at 500 °C. Once again, the temperature range, which corresponds to the departure of water or hydroxyls, makes the analysis difficult.

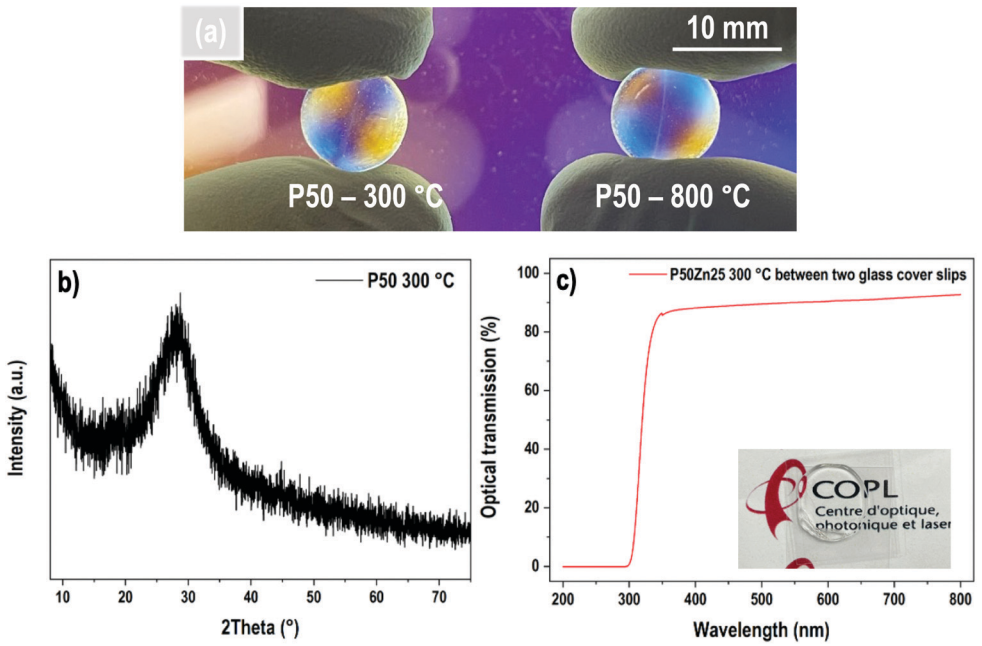

Fig. 2 (a) Transparent P50 samples prepared at 300 °C and 800 °C; (b) X-ray diffractogram of P50 glass and (c) its optical transmission obtained between two glass cover slips.

Table 2 Evolution of the estimated compositions with temperature for the P50 and P50Zn25 compositions

		Estimated content (±1 mol%)					
Composition	T (°C)	P_2O_5	K_2O	Na_2O	ZnO	H_2O	O/P ratio
P50	300	30	15	15	0	40	3.67
	500	48	24	24	0	4	3.04
	800	>49	>25	>25	0	<1	3.02
P50Zn25	300	33	9	9	17	32	3.51
	500	46	12	12	23	7	3.09
	800	>50	>12	>12	>25	<1	3.00

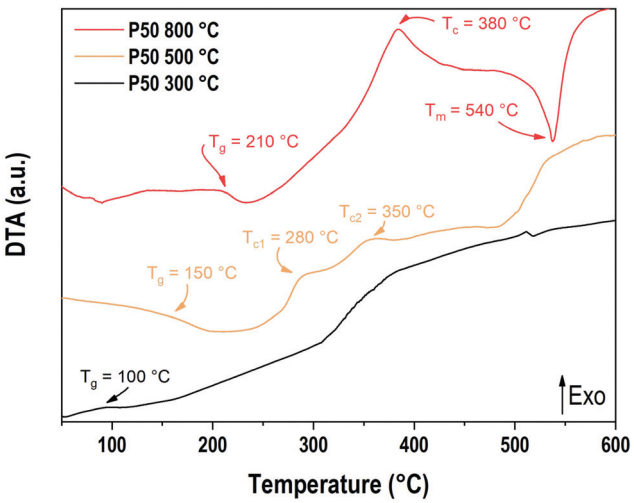

Fig. 3 DTA curves of P50 samples prepared at 300 °C, 500 °C and 800 °C.

The evolution of the material densities with ZnO content for samples prepared at 300 °C and 800 °C is presented in Fig. 4. For both series of samples, the density follows a linear growth. For the samples prepared at 300 °C, the density increases from 2.37 g cm^{-3} for the P50 composition to 2.60 g cm^{-3} for the P50Zn25 composition, while for the samples prepared at 800 °C, the density starts at 2.47 g cm^{-3} for the P50 composition and ends at 2.73 g cm^{-3} for the P50Zn25 composition. The difference between the two series is constant with the addition of ZnO. One can notice that, regardless of the zinc oxide amount, the increase of density between the materials fabricated at 300 °C and 800 °C is about 4.8%, implying a comparable structural and composition change.

The evolution of the refractive indices for P50Zn25 samples prepared at 300 °C, 500 °C and 800 °C is shown in Fig. 5. All series depict dispersion with the variation of wavelength, with the values of the refractive indices lowering as the wavelength increases. The evolution of the refractive indices with the wavelength follows a nonlinear trend which is expected to be in accordance with a Sellmeier model. The refractive indices for the samples prepared at 500 °C and 800 °C are nearly equal regardless of the wavelength (1.523 and 1.523 at 589 nm for the samples prepared at 500 °C and 800 °C, respectively), while the refractive index for the 300 °C series is significantly lower than its counterparts (1.518 at 589 nm). As with the evolution of density with addition of ZnO, the gap between the 300 °C series and the other series remains constant (+0.3%) regardless of the wavelength.

The inset in Fig. 5 reports the evolution of the linear susceptibility ($\chi^{(1)}$), calculated from the measured refractive index at 589 nm with the addition of ZnO. As already observed for the density, the $\chi^{(1)}$ increases linearly with the addition of

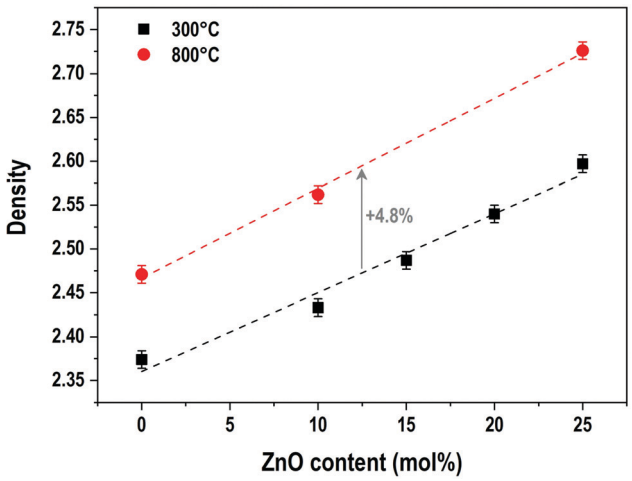

Fig. 4 Evolution of density with ZnO content for samples prepared at 300 °C and 800 °C.

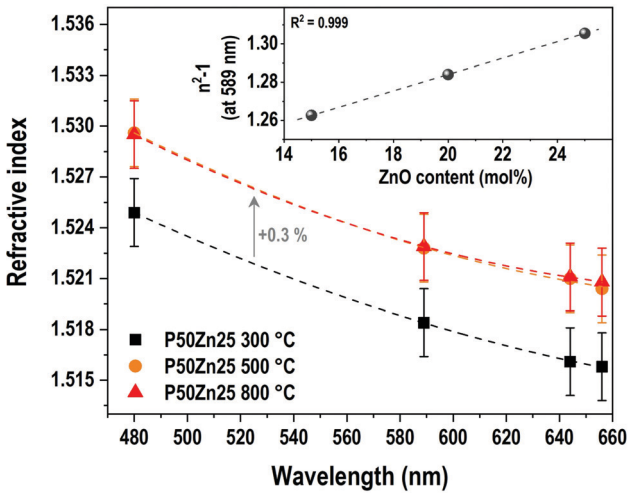

Fig. 5 Evolution of the refractive index with wavelength for P50Zn25 samples prepared at 300 °C, 500 °C and 800 °C. Lines are guides for the eyes. Inset: Evolution of the 1st order susceptibility term at 589 nm with ZnO content for samples prepared at 300 °C. Error bars are comprised in the symbols.

ZnO concentration, from 1.262 to 1.306 for both P50Zn15 and P50Zn25 compositions, respectively.

Vibrational spectroscopies

Vibrational spectroscopies have been conducted to investigate the structure of the materials. The analysis has been first conducted on the zinc-free P50 composition. Raman spectroscopy allows investigating the vibrational signature in the volume without deploying a polishing step which encounters difficulties for the sample obtained at 300 °C. Fig. 6 shows the Raman spectra in the range of 600 cm^{-1}–4000 cm^{-1} of the P50 composition prepared at three different temperatures. In the inset, the same spectra are depicted in the restricted 600–1400 cm^{-1} range. Large spectral variations are observed

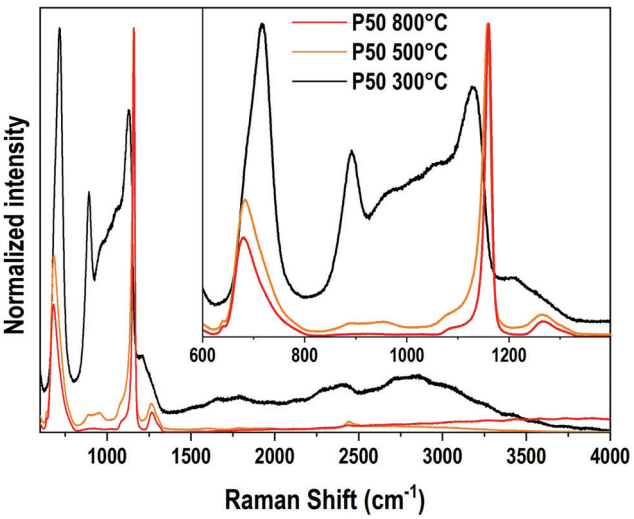

Fig. 6 Raman spectra of the P50 sample prepared at 300 °C, 500 °C and 800 °C. Inset: The same Raman spectra in the 600–1400 cm^{-1} range.

between the sample prepared at 300 °C and the two others obtained at higher temperatures. One should first notice in the high wavenumber domain (beyond 1400 cm^{-1}) the important convolution of multiple bands corresponding to either O–H bonds in phosphate units or free H_2O molecules as already reported in Raman or IR spectra of phosphate hydrated salts for instance.[12,29,30] This very large and complex spectral profile is not observed for both samples prepared at 500 °C and 800 °C which can be related to the dehydration of these glassy matrices. In a second time, we focus on the spectral range 800–1300 cm^{-1} linked to P–O stretching modes in various structural units. The sample P50 300 °C shows a large spectral profile formed by two predominant bands at 890 cm^{-1} and 1130 cm^{-1} and additional strong components peaking at 950 and 1050 cm^{-1}. For both samples prepared at 500 °C and 800 °C, one main contribution with a relatively sharp spectral profile appears at 1160 cm^{-1}. The corresponding assignments can be done based on spectroscopic investigations of binary phosphate glassy systems[31,32] and KH_2PO_4 (KDP) crystals.[33,34] The symmetric Raman active mode of orthophosphate units has been observed at 950 cm^{-1} in lithium phosphate glasses and the 900–930 cm^{-1} range for KDP. The symmetric stretching $\nu_s(PO_2^-)$ in Q^2 units was observed in the range of 1160–1200 cm^{-1} in various metaphosphate glassy compositions.[31,32] Finally, the symmetric stretching mode of the end groups of pyrophosphate Q^1 units $\nu_s(PO_3^{2-})$ is expected in the range of 1000–1050 cm^{-1}.[31,32] Thus, for the P50 composition prepared at 300 °C, the Raman spectrum indicates a very large variety of structural units in link with the observed vibrational signatures of ortho, pyro and metaphosphate structural entities. In addition, it is also noticed that the compensation of the phosphate network negative charges is done by both alkaline cations (Na^+, K^+) and hydroxyl groups, which should affect differently the strength of the P–O bonds and can explain the important broadening of the Raman modes measured for the P50 300 °C sample. Upon heating at 500 and 800 °C, the loss of water and hydroxyl groups induce

the formation of long metaphosphate chains for which both symmetric and asymmetric stretchings are observed at 1130 and 1270 cm^{-1}, respectively. Meanwhile, near the band associated with P–O–P symmetric stretching in the range of 680–750 cm^{-1}, a change in its spectral profile is observed as expected by the large changes in phosphate structural units induced by the increase in the synthesis temperature. Finally, for the glass synthesized at 500 °C, additional weak contributions at about 890 cm^{-1} and 960 cm^{-1} are observed and attributed to the remaining Q^0 species as already mentioned for the 300 °C-prepared sample.

The effect of substitution of alkali oxides by zinc oxide was followed by Raman and FTIR spectroscopies. The IR absorption coefficient signal could not be collected from the P50 composition due to the difficulty of the polishing steps and the hygroscopicity of the sample. In the samples with 15, 20 and 25 mol% of ZnO, comparable overall envelopes of IR spectra are observed in Fig. 7a. These spectra are composed of a wideband convolution between 700 cm^{-1} and 1250 cm^{-1}, with major peaks located at 920 cm^{-1}, 970 cm^{-1}, 1100 cm^{-1} and 1220 cm^{-1}. More precisely, the band at 1220 cm^{-1} is a convolution of two bands at 1200 cm^{-1} and 1270 cm^{-1}.

In IR, the asymmetric stretching $\nu_s(PO_4^{3-})$ of Q^0 units is attributed to the band at 970 cm^{-1}.[33–36] The contributions at 1100 cm^{-1} corresponds to the mode $\nu_{as}(PO_3^{2-})$ of Q^1 entities,[32,33,36] while the ones at 1200 and 1270 cm^{-1} are assigned to symmetric and asymmetric PO_2^- stretching modes in Q^2 species.[31,37] The vibrational modes linked to P–O–P bridges in Q^1 dimers or Q^2 chains are observed at 740 and 920 cm^{-1} for ν_s and ν_{as}(P–O–P) stretching modes, respectively. In the higher wavenumber domain (>1400 cm^{-1}), contributions are assigned to OH bonds, whether it is in free water molecules or $H_2PO_4^-$ ionic groups.[12,29,30]

By increasing the ZnO content, beyond 1400 cm^{-1}, no significant modifications are observable, except for the domain at 3640 cm^{-1} which is strongly dependent on the glass surface hydration. The higher the zinc incorporation, the smaller the 3640 cm^{-1} band intensity. This latter observation seems to indicate a weaker and/or slower hydration of the glass surface thanks to the zinc introduction. Concerning the phosphate network, few structural modifications are denoted. Both 1200 and 1100 cm^{-1} contributions appear more noticeable which could indicate a relative increase in the number of Q^1 and Q^2 units as compared to orthophosphate entities.

The Raman spectra of P50 and P50Zn25 samples prepared at 300 °C and 800 °C are reported in Fig. 7b. Whether at 300 °C or 800 °C, the incorporation of zinc oxide leads to broadening of most of the contributions and shifting their maximum position towards higher wavenumbers. This is an indication of the role of zinc in the charge compensation of the phosphate network.[31]

The IR absorption coefficient spectra of P50Zn25Eu samples prepared at 300 °C, 500 °C and 800 °C are reported in Fig. 8. Compared to the IR spectrum of the P50Zn25 synthesized at 300 °C described in the previous section, the incorporation of 0.1 mol% of europium(III) oxide (P50Zn25Eu) does not affect

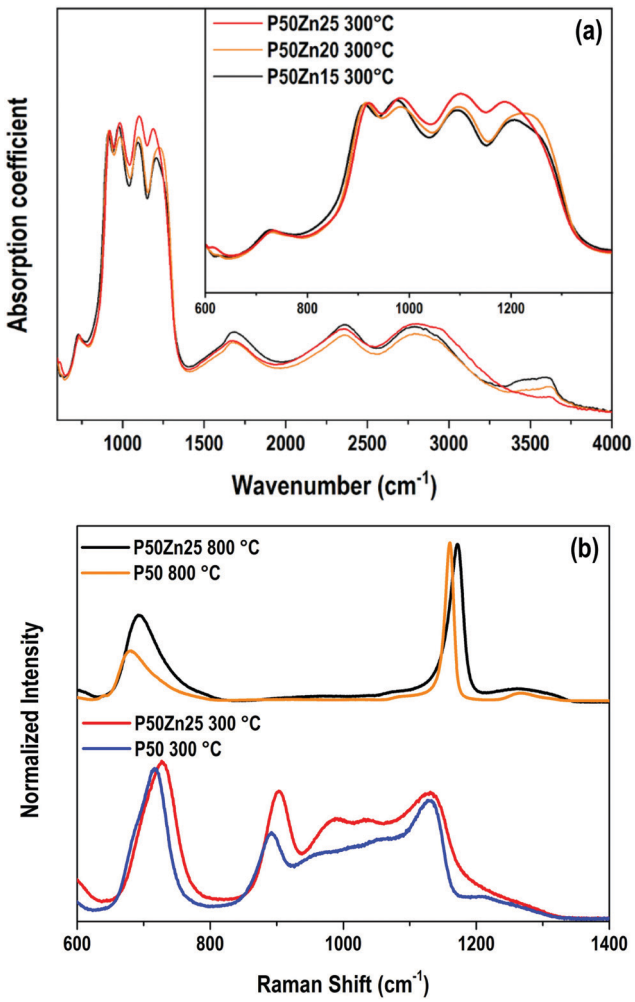

Fig. 7 (a) Absorption coefficient (α) spectra of samples P50Zn15, P50Zn20 and P50Zn25 prepared at 300 °C in the 600–4000 cm^{-1} range. Inset: Absorption coefficient spectra in the 600–1400 cm^{-1} range. (b) Raman spectra of samples P50 and P50Zn25 prepared at 300 °C and 800 °C in the 600–1400 cm^{-1} range.

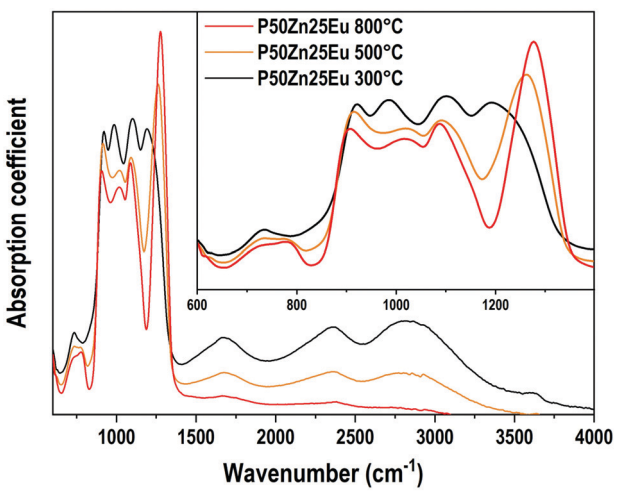

Fig. 8 Absorption coefficient (α) spectra of P50Zn25Eu samples prepared at 300 °C, 500 °C and 800 °C in the 600-4000 cm^{-1} range. Inset: Absorption coefficient spectra in the 600–1400 cm^{-1} range.

the absorption coefficient spectrum feature. From the amorphous material prepared at 300 °C, the glass fabricated at 500 and 800 °C highlights important progressive losses of all the bands above 1500 cm^{-1}, which is linked to the presence of hydroxyl groups and water in the glassy network, as observed in the Raman spectra in Fig. 6. For the phosphate network, the Q^0 bands at 970 cm^{-1} vanished, revealing two contributions at 900 cm^{-1} and 1020 cm^{-1} assigned respectively to asymmetric P–O–P stretching modes in Q^2 units and Q^1 entities.[32] Meanwhile, a significant increase and a shift to higher wavenumbers of the $\nu_{as}(PO_2^-)$ Q^2 mode are observed to be the main contribution at 1270 cm^{-1}.

The emission spectra (λ_{ex} = 532 nm) of the europium ions in the Eu-doped P50Zn25 samples prepared at 300 °C, 500 °C and 800 °C are reported in Fig. 9. In all spectra, the following features are observed: a weak peak at 578 nm, a multiplet of medium intensity from 585 to 600 nm with distinct peaks at 588 nm, 592 nm, and 594 nm, a multiplet from 610 to 625 nm with an intense and narrow peak located at 611 nm, and a weak multiplet from 647 to 658 nm. These broad emissions correspond respectively to the $^5D_0 \rightarrow {}^7F_0$, $^7F_1$, $^7F_2$ and $^7F_3$ 4f–4f transitions of europium(III) ions in an amorphous environment exhibiting an inhomogeneous broadening. Given the high sensitivity of the europium ion's luminescence signature to its surrounding environment, europium ions can be considered as a structural probe. Indeed, the luminescence properties and in particular the 4f–4f transitions corresponding to the transition $^5D_0 \rightarrow {}^7F_2$ (red emission) and the $^5D_0 \rightarrow {}^7F_1$ (orange emission) having different selection rules (respectively electric dipole and magnetic dipole transitions) allows retrieving information on the environment of the rare earth ion. Indeed, the $^5D_0 \rightarrow {}^7F_1$ magnetic dipole transition scarcely varies with the crystal-field strength surrounding europium(III) ions and its site symmetry, whereas the $^5D_0 \rightarrow {}^7F_2$ hypersensitive electric dipole transition does. Such hypersensitive electric dipole transition is deeply affected by the electronegativity of the oxygens around the Eu^{3+} ions, leading to an enhancement of its fluorescence amplitude when either the oxygens become less ionic, more covalent[38] and/or the europium symmetry is lower.[39]

In the Eu^{3+}-doped phosphate glasses of this study, the $^5D_0 \rightarrow {}^7F_2/{}^5D_0 \rightarrow {}^7F_1$ emission ratios increase slightly with the increase of the material fabrication temperature while the emission profile of the three transitions $^5D_0 \rightarrow {}^7F_0$, $^5D_0 \rightarrow {}^7F_1$ and $^5D_0 \rightarrow {}^7F_2$ remains constant. Such a phenomenon indicates that the europium(III) ions conserve predominantly the same site independently of the synthesis temperature. Hence, only a slight change of the bond covalence or a slight distortion of the rare-earth oxygenated site can be proposed.

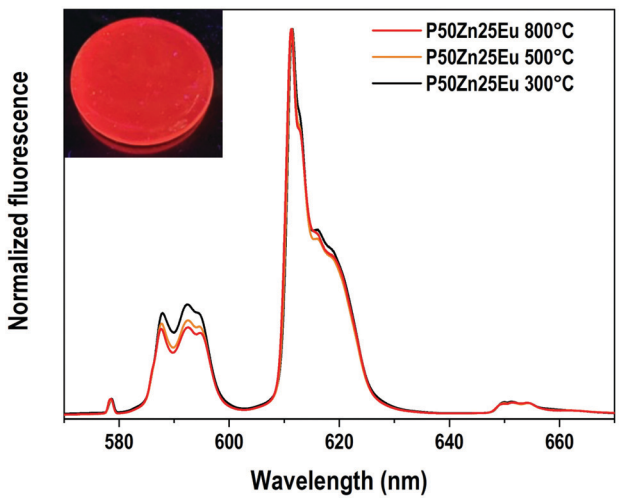

Fig. 9 Normalized emission spectra (λ_{exc} = 532 nm) for Eu-doped P50Zn25 samples prepared at 300 °C, 500 °C and 800 °C. Inset: The Eu-doped P50Zn25 sample prepared at 300 °C under UV light (λ_{exc} = 325 nm).

Conclusions

In this work, transparent amorphous hydrated phosphate materials were synthesized at 300 °C and compared to glasses of the same compositions prepared at 500 °C and 800 °C. The molar water content in the hydrated phosphates has been estimated between 30 and 40 mol% by TGA. Raman and FTIR spectroscopies suggest that the structure of the hydrated phosphates consists of short phosphate chains, analogous to pyrophosphates, linked by hydrogen bonds, while glasses of the same composition and prepared at higher temperatures tend towards a polyphosphate structure. Further analyses, such as ^{1}H-NMR and ^{31}P-NMR, will provide complementary information on the structure of hydrated phosphates, and are currently in progress. The properties of the hydrated phosphates are also significantly altered by the presence of hydroxyl bonds in the structure. Europium(III) luminescence spectra are barely affected by the synthesis temperature, meaning the Eu^{3+} ions are in stable sites between the phosphate chains. Zinc oxide addition does not seem to significantly influence the structure of the materials, as the O/P ratio and IR spectra are unchanged between the different compositions. Hence, these novel hydrated phosphate materials appear as potential candidates for developing new routes of glass-based composite materials through their functionalization with compatible compounds having a degradation temperature above 300 °C.

Conflicts of interest

There are no conflicts to declare.

Acknowledgements

This project has received funding from the European Union's Horizon 2020 research and innovation program under the Marie–Skłodowska–Curie grant agreement N°823941 (FUNGLASS). Funding for this work has been provided by the French Government, managed by the French National Research Agency (ANR-17-CE08-0042-01) and the Nouvelle Aquitaine Region, and from the Canadian Government, managed by Sentinel North

program of University Laval and the Canadian Excellence Research Chair program (CERC).

Notes and references

1 W. Liu, J. Sanz, C. Pecharromán, I. Sobrados, S. Lopez-Esteban, R. Torrecillas, D.-Y. Wang, J. S. Moya and B. Cabal, *Ceram. Int.*, 2019, **45**, 12234–12242.
2 A. Lapa, M. Cresswell, P. Jackson and A. R. Boccaccini, *Adv. Appl. Ceram.*, 2020, **119**, 1–14.
3 R. M. Zaki, C. Strutynski, S. Kaser, D. Bernard, G. Hauss, M. Faessel, J. Sabatier, L. Canioni, Y. Messaddeq, S. Danto and T. Cardinal, *Mater. Des.*, 2020, **194**, 108957.
4 R. K. Brow, *J. Non-Cryst. Solids*, 2000, **263–264**, 1–28.
5 E. Popova and Y. Dimitriev, *J. Mater. Sci.*, 2007, **42**, 3358–3366.
6 H. Masai, N. Toru, S. Yamamoto, T. Niizuma, N. Kitamura, T. Akai, T. Ohkubo and M. Yoshida, *Sci. Rep.*, 2021, **11**, 214.
7 C. Sanchez, L. Rozes, F. Ribot, C. Laberty-Robert, D. Grosso, C. Sassoye, C. Boissiere and L. Nicole, *C. R. Chim*, 2010, **13**, 3–39.
8 R. Backov, *Soft Matter*, 2006, **2**, 452.
9 L. Mayen, N. D. Jensen, D. Laurencin, O. Marsan, C. Bonhomme, C. Gervais, M. E. Smith, C. Coelho, G. Laurent, J. Trebosc, Z. Gan, K. Chen, C. Rey, C. Combes and J. Soulié, *Acta Biomater.*, 2020, **103**, 333–345.
10 J. Livage, *Curr. Opin. Solid State Mater. Sci.*, 1997, **2**, 132–138.
11 A. E. Danks, S. R. Hall and Z. Schnepp, *Mater. Horiz.*, 2016, **3**, 91–112.
12 K. A. Syed, S.-F. Pang, Y. Zhang and Y.-H. Zhang, *J. Chem. Phys.*, 2013, **138**, 024901.
13 M. Badrouj and R. Malekfar, *J. Raman Spectrosc.*, 2007, **38**, 1089–1096.
14 N. Balamurugan and P. Ramasamy, *Cryst. Growth Des.*, 2006, **6**, 1642–1644.
15 N. P. Zaitseva, J. J. De Yoreo, M. R. Dehaven, R. L. Vital, K. E. Montgomery, M. Richardson and L. J. Atherton, *J. Cryst. Grow.*, 1997, **180**, 255–262.
16 S. Bach, V. R. Celinski, M. Dietzsch, M. Panthöfer, R. Bienert, F. Emmerling, J. Schmedt auf der Günne and W. Tremel, *J. Am. Chem. Soc.*, 2015, **137**, 2285–2294.
17 M. Maslyk, S. Bach, W. Li, S. I. Shylin, M. Panthöfer, B. Barton, V. Ksenofontov, K. Xu, B. Meermann, U. Kolb, J. Schmedt auf der Günne and W. Tremel, *J. Phys. Chem. C*, 2021, **125**, 2636–2647.
18 P. Sikder, C. R. Grice, B. Lin, V. K. Goel and S. B. Bhaduri, *ACS Biomater. Sci. Eng.*, 2018, **4**, 2767–2783.
19 K. Raju, H. Han, D. B. Velusamy, Q. Jiang, H. Yang, F. P. Nkosi, N. Palaniyandy, K. Makgopa, Z. Bo and K. I. Ozoemena, *ACS Energy Lett.*, 2020, **5**, 23–30.
20 M. Dompé, F. J. Cedano-Serrano, O. Heckert, N. van den Heuvel, J. van der Gucht, Y. Tran, D. Hourdet, C. Creton and M. Kamperman, *Adv. Mater.*, 2019, **31**, 1808179.
21 W. C. Blocher and S. L. Perry, *Wiley Interdiscip. Rev.: Nanomed. Nanobiotechnol.*, 2017, **9**, DOI: 10.1002/wnan.1442.
22 F. Foroutan, A. Nikolaou, B. A. Kyffin, R. M. Elliott, M. Felipe-Sotelo, J. Gutierrez-Merino and D. Carta, *Materialia*, 2020, **14**, 100939.
23 J. R. Orives, W. R. Viali, S. H. Santagneli, C. R. M. Afonso, M. H. Carvalho, A. J. A. de Oliveira and M. Nalin, *Dalton Trans.*, 2018, **47**, 5771–5779.
24 G. Palavit, L. Montagne and R. Delaval, *J. Non-Cryst. Solids*, 1995, **189**, 277–282.
25 A. M. Nepomiluev, R. N. Pletnev, O. B. Lapina, S. G. Kozlova and V. G. Bamburov, *Glass Phys. Chem.*, 2002, **28**, 1–4.
26 C. Mercier, L. Montagne, H. Sfihi, G. Palavit, J. C. Boivin and A. P. Legrand, *J. Non-Cryst. Solids*, 1998, **224**, 163–172.
27 D. Ehrt, *J. Non-Cryst. Solids*, 2008, **354**, 546–552.
28 A. Faivre, F. Despetis, L. Duffours and P. Colombel, *Int. J. Appl. Glass Sci.*, 2019, **10**, 162–171.
29 V. Koleva and H. Effenberger, *J. Solid State Chem.*, 2007, **180**, 956–967.
30 C. Dayanand, G. Bhikshamaiah, V. Jaya Tyagaraju, M. Salagram and A. S. R. Krishna Murthy, *J. Mater. Sci.*, 1996, 1945–1967.
31 R. K. Brow, D. R. Tallant, S. T. Myers and C. C. Phifer, *J. Non-Cryst. Solids*, 1995, **191**, 45–55.
32 L. L. Velli, C. P. E. Varsamis, E. I. Kamitsos, D. Möncke and D. Ehrt, in Structural investigation of metaphosphate glasses, *Phys. Chem. Glasses*, 2005, **46**, 178–181Athens, Greece, 25–28 April 2004.
33 C. M. Preston and W. A. Adams, *J. Phys. Chem.*, 1979, **83**, 814–821.
34 M. K. Cerreta and K. A. Berglund, *J. Cryst. Growth*, 1987, **84**, 577–588.
35 V. Koleva and V. Stefov, *Vib. Spectrosc.*, 2013, **64**, 89–100.
36 M. Dussauze, E. I. Kamitsos, E. Fargin and V. Rodriguez, *J. Phys. Chem. C*, 2007, **111**, 14560–14566.
37 K. Meyer, *J. Non-Cryst. Solids*, 1997, **209**, 227–239.
38 M. Nogami, N. Umehara and T. Hayakawa, *Phys. Rev. B: Condens. Matter Mater. Phys.*, 1998, **58**, 6166–6171.
39 K. Swapna, Sk Mahamuda, A. S. Rao, T. Sasikala, P. Packiyaraj, L. R. Moorthy and G. V. Prakash, *J. Lumin.*, 2014, **156**, 80–86.